3-30-2016

Dispersion of Electric-Field-Induced Faraday Effect in Magnetoelectric Cr2O3

J. Wang
University of Nebraska-Lincoln

Christian Binek
University of Nebraska-Lincoln, cbinek@unl.edu

PHYSICAL REVIEW APPLIED 5, 031001 (2016)

Dispersion of Electric-Field-Induced Faraday Effect in Magnetoelectric Cr_2O_3

Junlei Wang and Christian Binek

Department of Physics and Astronomy, University of Nebraska-Lincoln, Lincoln, Nebraska 68588, USA

(Received 12 October 2015; revised manuscript received 26 February 2016; published 30 March 2016)

The frequency dependence of the electric-field-induced magneto-optical Faraday effect is investigated in the magnetoelectric antiferromagnet chromia. Two electrically induced Faraday signals superimpose in proportion to the linear magnetoelectric susceptibility α and the antiferromagnetic order parameter η. The relative strength of these contributions is determined by the frequency of the probing light and can be tuned between extreme characteristics following the temperature dependence of α or η. The frequency dependence is analyzed in terms of electric dipole transitions of perturbed Cr^{3+} crystal-field states. The results allow us to measure voltage-controlled selection, isothermal switching, and temperature dependence of η in a tabletop setup. The voltage-specific Faraday rotation is independent of the sample thickness, making the method scalable and versatile down to the limit of dielectric breakdown.

DOI: 10.1103/PhysRevApplied.5.031001

Electric-field-induced Faraday rotation is a fascinating phenomenon in magnetoelectrics with antiferromagnetic (AFM) spin order. Little is known about the dispersion of this magneto-optical effect. Theory suggests that dispersion can be utilized to tune into a regime where the Faraday signal is proportional to the AFM order parameter η. Measuring the orientation of η is a notoriously difficult problem in condensed-matter physics. This is largely because perfect AFM spin order leads to vanishing net magnetization, thus, ruling out standard magnetometry as a characterization technique. Experiments discriminating two degenerate AFM 180° domains have proven challenging. This holds particularly in thin-film magnetism where AFM constituents allow for the potentially advantageous variation of AFM spintronics [1–3] or applications such as voltage-controlled ultra-low-power spintronics [4–6].

Established methods which allow the measurement of η include neutron diffraction, x-ray linear magnetic dichroism (XMLD), and optical second-harmonic generation. Both neutron diffraction and XMLD require large-scale research facilities. While neutron-diffraction topography suffers from the need of long exposure times [7], XMLD has other shortcomings. It senses spin alignment via charge distribution [8,9]. The situation has been improved with the advent of nonlinear optical topography first applied for the magnetoelectric (ME) antiferromagnet Cr_2O_3 (chromia) [10]. In ME antiferromagnets, time and spatial inversion symmetry are broken below the Néel temperature T_N. Their combined application leaves the AFM spin structure invariant [11]. These symmetry requirements allow for electric-field- (E-) induced magnetization $\mu_0 \underline{M} = \underline{\underline{\alpha}}\, \underline{E}$, where α is the ME susceptibility. Fiebig *et al.* [12] were able to generalize their method when relaxing the previously required symmetry constraints of ME antiferromagnets through extrinsic experimental refinements. This improvement makes second-harmonic generation a powerful method of topography. It lacks, however, the ability to determine the sign of η. In addition, all of the above methods are not suitable for investigations of thin-film samples.

In this Letter, we investigate the dc electric-field-induced Faraday effect (EFIF) and its dispersion. Specifically, the temperature (T) dependence of the Faraday rotation Θ of the ME antiferromagnet chromia is studied on variation of the frequency ω of the probing light. A fundamental insight gained from the analysis of $\Theta(T)$ for light frequencies $10\,000 < \omega < 12\,500\ \mathrm{cm}^{-1}$ is the ability to tune ω into a regime where $\Theta \propto \eta$. With this finding, we establish a compact method sensitive to measure the sign and magnitude of η in the ME antiferromagnet chromia and potentially other ME antiferromagnets [13]. Our results demonstrate dispersion of the EFIF and enable voltage-controlled selection, isothermal switching, and measurement of the T dependence of η. These capabilities have significance for the investigation of AFM spin structures and the development of applications aiming at voltage control of memory and logical states via switching of AFM domain states. Recently, nonvolatile ultra-low-power memory and logical devices have been proposed. They employ the ME effect and the associated voltage-controlled AFM order-parameter switching in thin-film heterostructures for virtually dissipationless switching of state variables. ME devices encode information in remnant and, thus, nonvolatile magnetization states providing additional functionality over CMOS counterparts. In ME devices, voltage-controlled nonlinear switching of boundary magnetization, a generic property of ME antiferromagnets [14–16], is mapped onto voltage-controlled switching between remnant magnetization of an adjacent ferromagnetic (FM) thin film through quantum-mechanical exchange at the AFM/FM interface. It gives rise to voltage-controlled exchange bias [15,17,18] enabling, e.g., ultra-low-power ME magnetic random-access memory, majority

gates, and other ME variations of memory and logic device applications [4,5].

The Faraday effect is, next to the Kerr effect, among the commonly exploited methods to characterize magnetic materials. The Faraday and Kerr effects are in the class of rare nonreciprocal optical phenomena [19,20]. Faraday rotation refers to the rotation of the polarization plane of linearly polarized light transmitted through a magnetized sample. ME antiferromagnets show an E-field-induced Faraday effect [21]. In contrast to ordinary Faraday rotation, EFIF takes place in the absence of an applied magnetic field or sample inherent magnetization. Two distinct mechanisms constitute the total E-field-induced rotation. These are the magnetization induced by the ME effect with a T dependence following $\alpha(T)$ and an E-field-induced pseudo-Stark effect, which creates rotation with a T dependence proportional to $\eta(T)$. The understanding of EFIF is best developed for the archetypical ME antiferromagnet Cr_2O_3 [11,21,22]. Despite the groundbreaking previous work, experimental investigations of dispersion of EFIF are still lacking, even in the archetypical Cr_2O_3. It is the prime objective of this work to fill in this gap. To bring our experiments in the context of the theoretical framework, we briefly recapitulate the phenomenology and microscopic origin of the EFIF [21].

EFIF, like all Faraday rotation, originates from the difference $\Delta n = n_+ - n_-$ in the refractive indices for positive (+) and negative (−) circularly polarized light. Δn can be traced back to the presence of complex off-diagonal elements in the dielectric tensor ϵ_{ij}. The elements $\epsilon_{xy} = -\epsilon_{yx}$ can be expressed as $\epsilon_{xy} = ig_z$, where g_z is the z component of the gyrotropic vector. In uniaxial ferromagnets with magnetization M along the z axis, Faraday rotation is proportional to M in accordance with $g_z \propto M$ and $g_z \ll \epsilon_{xx}$. In analogy to Faraday rotation in uniaxial ferromagnets, one expects for a uniaxial antiferromagnet with sublattice magnetizations $M_{A,B}$ that $g_z = 2(p_A M_A + p_B M_B)$, where z corresponds to the c axis in chromia. In $E_z = 0$, the coefficients $p_{A,B}$ are degenerate according to $p_A = p_B = p$. Because $M_B = -M_A$, in zero fields this perfect opposition of sublattice magnetizations yields vanishing Faraday rotation in antiferromagnets. Note that although η of chromia is composed from four sublattices [21], it is sufficient for our purpose to distinguish sites with up and down spins [21]. An applied electric field E_z induces $\Theta \neq 0$ in $H = 0$ for ME antiferromagnets such as chromia. In chromia, the E field displaces the Cr^{3+} ions along the threefold c axis moving them into different crystal-field environments. The dissimilar crystal field lifts the degeneracy of A (up spins) and B sites (down spins) resulting in $p_{A,B} = p \pm qE_z$ [21]. When eliminating $M_{A,B}$ in $g_z = 2(p_A M_A + p_B M_B)$ via $M_z = M_A + M_B = \alpha E_z$ and $\eta = M_A - M_B$, the z component of the gyrotropic vector reads $g_z = 2(p\alpha E_z + q\eta E_z)$. It provides the phenomenological functional form

$$\Theta = Kd(p\alpha E_z + q\eta E_z), \tag{1}$$

of EFIF, where K is a proportionality constant.

Microscopically, Faraday effects are based on electric dipole transitions [23]. From crystal-field theory of chromium trihalides and similar for chromia, it is known that an appreciable Faraday effect originates from the average dipole moment of d-d transitions [21,24]. In chromia, these are the transitions between the ground state $^4A_2$ and excited states of $^4T_2$ type of the Cr^{3+} ions. The $^4A_2$ and $^4T_2$ states split in the trigonal crystal field perturbed by spin-orbit interaction and exchange interaction. In addition, they experience a Stark-like shift in response to an applied E field [21]. Based on this crystal-field theory, the ω dependence of p and q has been worked out and reads

$$p(\omega) = \frac{2\pi\omega}{n\hbar c} p_\alpha^2 \left\{ \frac{1}{\omega_{C(\alpha)}^2 - \omega^2} - \sum_{i=1}^{3} \frac{a_{A_i(\alpha)}}{\omega_{A_i(\alpha)}^2 - \omega^2} \right\}, \tag{2}$$

$$q(\omega) = \frac{2\pi\omega}{n\hbar c} p_\alpha^2 \left\{ \frac{|A_1^0|(\chi_0 + \chi_C)}{(\omega_{C(\alpha)}^2 - \omega^2)^2} - \sum_{i=1}^{3} \frac{a_{A_i(\alpha)}^2 |A_1^0|(\chi_0 + \chi_{A_i})}{(\omega_{A_i(\alpha)}^2 - \omega^2)^2} \right\}, \tag{3}$$

where $\omega_{C(\alpha)}$ and $\omega_{A_i(\alpha)}$ are transition frequencies from the ground state to the states $C(\alpha) = C(m = \pm 5/2)$ and $A_{1,2,3}(\alpha) = A_{1,2,3}(m = \pm 1/2)$, respectively. Here, m is the quantum number of the z component of the angular momentum. The notation in Eqs. (2) and (3) is adopted from Ref. [21]. Specifically, $|A_1^0|(\chi_0 + \chi_{A_i})$ quantifies the pseudo-Stark splitting, i.e., a mere positive (negative) E-field-induced linear shift between the energy levels, of the levels of Cr^{3+} ions on the A (B) sides excited via circularly polarized light. Next, we provide an approximation for p/q using assumptions previously applied in Ref. [21]. Considering that the splitting of the $^4T_2$ level in the trigonal field is much greater than the spin-orbit splitting, it follows for the square of the transition-matrix elements $\alpha_{A_2}^2 \approx \alpha_{A_3}^2 \approx 0$. From the previous assumption that a mixing of wave functions is virtually identical for the most relevant excited states C and A follows $\chi_C \approx \chi_A$. With these approximations, p/q simplifies into

$$\frac{p(\omega)}{q(\omega)} = \frac{1}{|A_1^0|(\chi_0 + \chi_C)} \frac{(\omega_C^2 - \omega^2)(\omega_A^2 - \omega^2)}{\omega_A^2 - \omega^2 + a_{A_1}(\omega_C^2 - \omega^2)}. \tag{4}$$

We experimentally explore the ω dependence of Eq. (4) via spectroscopy of EFIF by utilizing laser light sources with wavelengths $\lambda = 804$, 830, 852, 905, 940, and 980 nm. The setup is shown in Fig. 1. We employ photoelastic modulation and a phase-sensitive lock-in technique to measure the EFIF effect. The polarization-modulated light is transmitted along the c axis of the chromia sample which resides in a custom-made ultra-high vacuum chamber with optical windows.

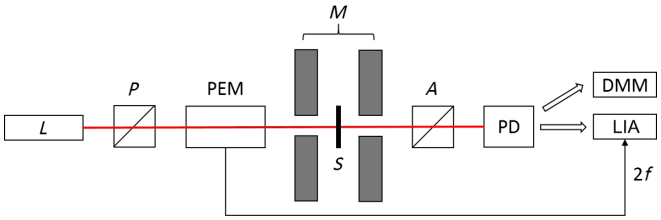

FIG. 1. Optical setup for EFIF effect. L, laser; P, polarizer; PEM, photoelastic modulator; M, electromagnet; S, sample inside ultra-high vacuum chamber; A, analyzer with automated rotational stage; PD, photodetector; DMM, digital multimeter; LIA, lock-in amplifier.

Prior to each measurement, the (0001)-oriented chromia single crystal, which has a semitransparent platinum electrode deposited on each (0001) surface, is prepared in an AFM single-domain state via ME annealing [25]. Electric ($E = \pm 3$ kV/mm) and magnetic fields ($\mu_0 H = \pm 150$ mT) are simultaneously applied along the [0001] direction (c axis) on cooling from $T = 340$ K $> T_N = 308$ K to $T = 280$ K $< T_N$. Cooling takes place at speed $|dT/dt| < 5$ K/min to avoid quenching into a multidomain state. ME annealing selects the registration of η through the sign of the sufficiently large EH product. At $T = 280$ K, when long-range AFM order has been established, fields are switched off and cooling continues in $E = H = 0$ to $T \approx 100$ K. Once the system equilibrates, EFIF is measured on heating.

Figure 2 shows a typical result of the T-dependent EFIF measured with laser light of $\lambda = 980$ nm. At each temperature, Θ vs applied voltage V is measured. dc electric fields $E = V/d$ are applied along the c axis through quasistatic variation of applied voltages within 50 V $< V <$ 1500 V where $d = 0.5$ mm is the thickness of the chromia single crystal. Note that our dc technique, although experimentally more challenging than ac techniques, has particular advantages. In a dc measurement, Θ vs V rather than $d\Theta/dV$ vs V is measured. Even though the implications of this fundamental difference are not further investigated in this Letter, it is worth mentioning that Θ vs V is free from dynamic anomalies and sensitive to V-independent Θ contributions. An important example is the Θ contribution originating from boundary magnetization which accompanies the bulk AFM order parameter in ME antiferromagnets [15,16]. The dc method has the capability to correlate boundary magnetization and η. A representative data set of a quasistatic Θ vs V measurement at $T = 250$ K is shown in the inset of Fig. 2. The Θ vs V isotherm determines the individual data point circled in the main panel of Fig. 2. In accordance with Eq. (1), Θ depends linearly on E and, thus, linearly on V. Hence, a linear best fit of Θ vs V provides the voltage-specific (Sp.) EFIF $d\Theta/dV$ according to

$$\frac{d\Theta}{dV} = \frac{d\Theta}{dE}\frac{dE}{dV} = K(p\alpha + q\eta). \tag{5}$$

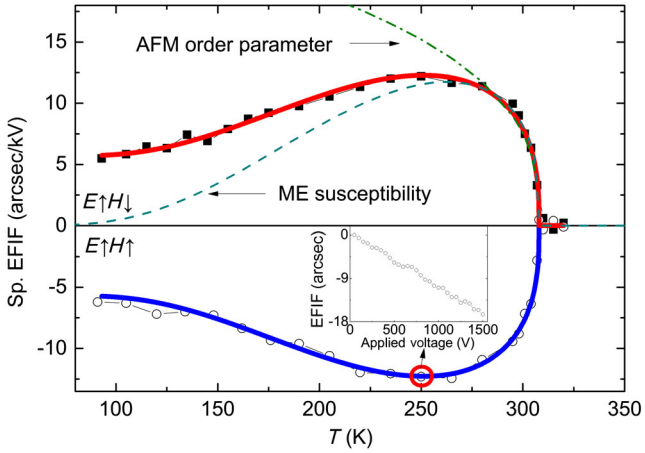

FIG. 2. Temperature dependence of the Sp. EFIF of Cr_2O_3 measured with light of 980-nm wavelength for the two degenerate AFM single-domain states with positive (squares) and negative (circles) η selected via field cooling in $EH < 0$ and $EH > 0$. Solid lines show best fits of Eq. (5). Dashed line shows contribution proportional to $\alpha(T)$. Dot-dashed line shows component proportional to $\eta(T)$. The inset displays EFIF as a function of applied voltage measured at $T = 250$ K.

Note that $d\Theta/dV$ is a thickness-independent-specific Faraday rotation. Invariance of $d\Theta/dV$ with respect to thickness scaling makes this method suitable for thin-film investigations, provided the dielectric properties of the films allow maintaining voltages similar to those applied in the bulk single crystal. While high voltages at the nanoscale are out of reach, electric fields in excess of 250 kV/mm have been applied across chromia (0001) films corresponding to voltages >100 V for films of <500 nm thickness [17,18]. The squares and circles in Fig. 2 show $d\Theta/dV$ vs T for the two distinct 180° single-domain states selected by respective ME annealing in $EH < 0$ (squares) and $EH > 0$ (circles). The two data sets show virtually perfect mirror symmetry relative to the T axis, reflecting the fact that both α and η flip sign when switching from one AFM single-domain state to the degenerate other. The prominent cutoff behavior in $d\Theta/dV$ vs T given by $d\Theta/dV = 0$ for $T > T_N$ indicates that $\alpha = \eta = 0$ above T_N. This T-dependence is in accordance with the necessary condition that EFIF requires broken time inversion symmetry as a result of spontaneous symmetry breaking accompanying the second-order AFM to paramagnetic phase transition.

The solid lines in Fig. 2 are least-squares fits of Eq. (5) to the $d\Theta/dV$ vs T data. In order to convert Eq. (5) into an explicit T-dependent function, we employ $\eta(T) = \eta_0(T_N - T)^\beta$ with $\beta = 0.355$ (Fig. 2 dot-dashed line) [26]. To obtain a parameter-free function for $\alpha(T)$, we employ the phenomenological product representation $\alpha = \alpha_0\eta(T)\chi(T)$ of the parallel ME susceptibility [27]. Here, α_0 is a constant, and $\chi(T)$ is the parallel magnetic susceptibility. We use an analytic approximation given by the

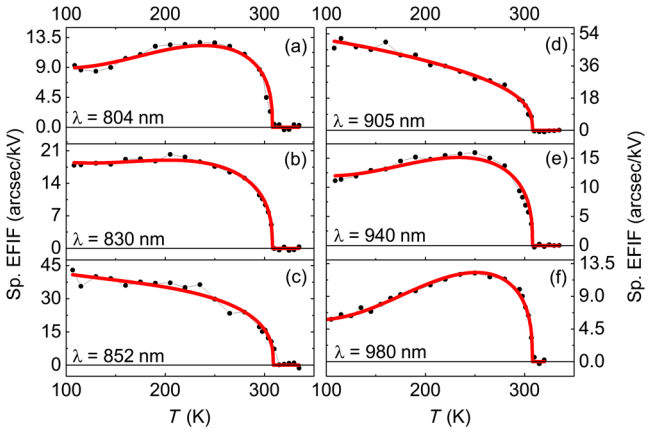

FIG. 3. Temperature dependence of Sp. EFIF probed with light at (a) 804, (b) 830, (c) 852, (d) 905, (e) 940, and (f) 980 nm, respectively. Circles represent data points obtained from isothermal EFIF measurements, respectively. Solid lines show best fits of Eq. (5). Respective ratios of the two free-fitting parameters are summarized in Table I.

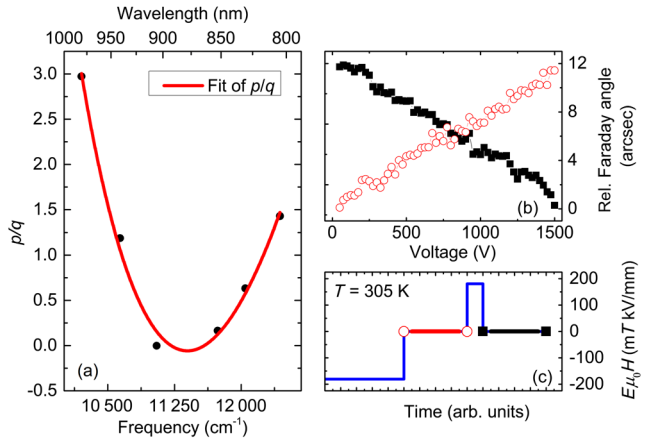

FIG. 4. (a) Ratio of the fitting parameters p/q as a function of frequency (wavelength) of the probing light. Solid line is the best fit of Eq. (4). (b) Isothermal Θ vs V data measured at $T = 305$ K following the field protocol shown in (c), which results in switching of η between $\eta > 0$ (circles) and $\eta < 0$ (squares).

Firgau formula, which is exact for Ising models on a Bethe lattice. The Firgau approximation is of sufficient accuracy because details of the criticality leave the global T dependence of the EFIF virtually unaffected [28,29]. The analytic expression $\alpha(T) = \alpha_0\eta(T)\chi(T)$ is fitted to experimental data of the ME susceptibility measured by Borisov *et al.* [30] with the help of a modified ac superconducting quantum-interference device method of high accuracy and precision [30]. The result of this fit is shown in Fig. 2 (dashed line). It becomes a parameter-free input for the least-squares fit of Eq. (5) to our Sp. EFIF data. The least-squares fit of Eq. (5) involves the free parameters $P_1 = K \cdot p$ and $P_2 = K \cdot q$. The results show perfect agreement with our data within their noise level. The fit allows decomposition of $d\Theta/dV$ vs T for each wavelength into the ME and the order-parameter component, respectively. The components provide the ratio p/q.

Figures 3(a)–3(f) show the $d\Theta/dV$ vs T data and corresponding best fits for $\lambda = 804$, 830, 852, 905, 940, and 980 nm, respectively. The resulting ratios p/q of the least-squares fits are summarized in Table I and plotted in Fig. 4(a) (circles) as functions of light frequency (and wavelength). We fit the data points using Eq. (4) to determine $\omega_C = 11\,584$ cm^{-1}, $\omega_A = 11\,213$ cm^{-1}, and the value of the matrix element $a_{A_1} = -0.904$. The results of the best fits agree with the assumptions $\omega_C \approx \omega_A$ and $|a_{A_1}| \sim 1$. The latter is in accordance with $\alpha_{A_2}^2 \approx \alpha_{A_3}^2 \approx 0$ due to the constraint $\alpha_{A_1}^2 + \alpha_{A_2}^2 + \alpha_{A_3}^2 = 1$.

The frequency dependence of p/q shown in Fig. 4(a) implies $p/q \to 0$ for light frequencies near $\omega = 11\,050$ cm^{-1} ($\lambda = 905$ nm). Here, the EFIF is directly proportional to η, as reflected by the order-parameter characteristics of $d\Theta/dV$ vs T in Fig. 3(d). It is interesting to note that $d\Theta/dV$ maximizes at $\lambda = 905$ nm (see Fig. 3) together with the minimizing of p/q. This correlation is consistent with the crystal-field theory predicting large Faraday rotation near the same d-d transitions which determine the dispersion of the EFIF. It is tempting to assume that the transition frequencies entering Eq. (4) can be inferred from the optical absorption spectrum measured in Ref. [31] in $E = 0$. However, it is important to keep in mind that the pseudo-Stark shift has a drastic but hitherto ill-quantified effect on ω_C and ω_A as reported in Refs. [21,32]. It prevents a quantitative comparison between our fitting results and the spectroscopy in $E = 0$. The possibility to tune into the regime where the T dependence of $d\Theta/dV$ is solely determined by $\eta(T)$ makes electric-field-induced Faraday rotation an ideal tool to study the AFM order parameter. Additionally, EFIF, in general, is a tabletop technique to distinguish the two 180° AFM single-domain states, not just as a domain contrast but in terms of the sign of η of an individual AFM single domain. Of particular interest is monitoring isothermal switching of η shown in Fig. 4(b). An AFM single-domain state with $\eta > 0$ has been selected via ME annealing from $T = 340$ to 305 K in $E = 1.6$ kV/mm and $\mu_0 H = -110$ mT. After annealing [see Fig. 4(c) for

TABLE I. Summary of the fitting result.

Wavelength (nm)	804	830	852	905	940	980
Frequency (cm^{-1})	12 437.8	12 048.2	11 737.1	11 049.7	10 638.3	10 204.1
p/q	1.429	0.633	0.165	−0.001	1.188	2.974

protocol], the fields are removed, and Θ vs V is measured isothermally [circles in Fig. 4(b)]. The positive slope of Θ vs V indicates that annealing selected an AFM single-domain state with $\eta > 0$. Next, the sample is exposed at $T = 305$ K to an axial field product $EH > 0$ within $E = 1.6$ kV/mm and $\mu_0 H = +110$ mT resulting in a Θ vs V isotherm of negative slope [squares in Fig. 4(b)]. The change in slope is indicative of isothermal switching into a single-domain state with $\eta < 0$.

Gyrotropic birefringence has been proposed to measure η in chromia. However, the difference in rotation of the indicatrix associated with the AFM order and the resulting contribution to the birefringence are small and plagued by parasitic background signals hampering any attempt to quantitatively investigate $\eta(T)$ [22]. In contrast, the simplicity and scalability of EFIF opens the unique possibility to employ the method for technologically relevant AFM thin films.

In conclusion, we investigate dispersion of the electric-field-induced Faraday effect in the magnetoelectric antiferromagnet Cr_2O_3 and experimentally verify the frequency dependence predicted in the framework of a crystal-field theory. Our spectroscopic data confirm that the Faraday signal is composed of two electric-field-induced components, which exhibit the temperature dependence of the magnetoelectric susceptibility and the antiferromagnetic order parameter of Cr_2O_3. We demonstrate that the two contributions depend dissimilarly on the frequency of the probing light and analyze our data in the framework of electric dipole transitions between crystal-field states of the magnetic Cr^{3+} ion. We demonstrate that selection of the laser light frequency allows tuning into a regime where the specific Faraday rotation is directly proportional to the antiferromagnetic order parameter. This capability enables a convenient, tabletop approach to measure the antiferromagnetic order parameter and its switching, e.g., by pure electrical means. The implications range from domain topography, to reference-free measurement of the orientation of the antiferromagnetic order parameter, to measurements of its isothermal switching. Voltage-controlled switching of the antiferromagnetic spin structure enables spintronic devices such as ultra-low-power magnetic random-access memories, majority gates, and logical devices. Understanding of the voltage-induced reversal of the order parameter in magnetoelectric antiferromagnets is of key importance to advance this promising branch of voltage-controlled spintronics.

This project was supported by the Nanoelectronics Research Corporation (NERC), a wholly-owned subsidiary of the Semiconductor Research Corporation (SRC), through the Center for Nanoferroic Devices (CNFD), an SRC-NRI Nanoelectronics Research Initiative Center under Task IDs 2398.001 and 2587.001, by C-SPIN, one of six centers of STARnet, a SRC program, sponsored by MARCO and DARPA, and by NSF through Nebraska MRSEC Grant No. DMR-1420645. The research was performed in part in the Nebraska Nanoscale Facility, Nebraska Center for Materials and Nanoscience, which is supported by the National Science Foundation under Award NNCI: 1542182, and the Nebraska Research Initiative.

[1] Z. Wei, A. Sharma, A. S. Nunez, P. M. Haney, R. A. Duine, J. Bass, A. H. MacDonald, and M. Tsoi, Changing Exchange Bias in Spin Valves with an Electric Current, Phys. Rev. Lett. **98**, 116603 (2007).

[2] X. Marti, I. Fina, and T. Jungwirth, Prospect for antiferromagnetic spintronics, IEEE Trans. Magn. **51**, 1 (2015).

[3] E. V. Gomonay and V. M. Loktev, Spintronics of antiferromagnetic systems (review article), Low Temp. Phys. **40**, 17 (2014).

[4] P. A. Dowben, C. Binek, and D. E. Nikonov, in *Nanoscale Silicon Devices*, edited by S. Oda and D. K. Ferry (CRC Press, Boca Raton, FL, 2015).

[5] C. Binek and B. Doudin, Magnetoelectronics with magnetoelectrics, J. Phys. Condens. Matter **17**, L39 (2005).

[6] W. Kleemann and C. Binek, in *Magnetic Nanostructures*, edited by H. Zabel and M. Farle (Springer, Berlin 2013), p. 163.

[7] J. Baruchel, M. Schlenker, and W. L. Roth, Observation of antiferromagnetic domains in nickel-oxide by neutron-diffraction topography, J. Appl. Phys. **48**, 5 (1977).

[8] P. Kuiper, B. G. Searle, P. Rudolf, L. H. Tjeng, and C. T. Chen, X-Ray Magnetic Dichroism of Antiferromagnet Fe_2O_3: The Orientation of Magnetic Moments Observed by Fe $2p$ X-Ray Absorption Spectroscopy, Phys. Rev. Lett. **70**, 1549 (1993).

[9] M. M. Schwickert, G. Y. Guo, M. A. Tomaz, W. L. O'Brien, and G. R. Harp, X-ray magnetic linear dichroism in absorption at the L edge of metallic Co, Fe, Cr, and V, Phys. Rev. B **58**, R4289 (1998).

[10] M. Fiebig, D. Fröhlich, G. Sluyterman, v. L, and R. V. Pisarev, Domain topography of antiferromagnetic Cr_2O_3 by second-harmonic generation, Appl. Phys. Lett. **66**, 2906 (1995).

[11] T. H. O'Dell and E. A. D. White, Electric field induced Faraday rotation in chromic oxide, Philos. Mag. **22**, 649 (1970).

[12] M. Fiebig, D. Fröhlich, S. Leute, and R. V. Pisarev, Topography of antiferromagnetic domains using second harmonic generation with an external reference, Appl. Phys. B **66**, 265 (1998).

[13] J. Wang, J. A. Santana, N. Wu, C. Karunakaran, J. Wang, P. A. Dowben, and C. Binek, Magnetoelectric Fe_2TeO_6 thin films, J. Phys. Condens. Matter **26**, 055012 (2014).

[14] N. Wu, X. He, A. L. Wysocki, U. Lanke, T. Komesu, K. D. Belashchenko, C. Binek, and P. A. Dowben, Imaging and Control of Surface Magnetization Domains in a Magnetoelectric Antiferromagnet, Phys. Rev. Lett. **106**, 087202 (2011).

[15] X. He, Y. Wang, N. Wu, A. N. Caruso, E. Vescovo, K. D. Belashchenko, P. A. Dowben, and C. Binek, Robust

isothermal electric control of exchange bias at room temperature, Nat. Mater. **9**, 579 (2010).

[16] K. D. Belashchenko, Equilibrium Magnetization at the Boundary of a Magnetoelectric Antiferromagnet, Phys. Rev. Lett. **105**, 147204 (2010).

[17] K. Toyoki, Y. Shiratsuchi, A. Kobane, C. Mitsumata, Y. Kotani, T. Nakamura, and R. Nakatani, Magnetoelectric switching of perpendicular exchange bias in Pt/Co/α-Cr_2O_3/Pt stacked films, Appl. Phys. Lett. **106**, 162404 (2015).

[18] T. Ashida, M. Oida, N. Shimomura, T. Nozaki, T. Shibata, and M. Sahashi, Isothermal electric switching of magnetization in Cr_2O_3/Co thin film system, Appl. Phys. Lett. **106**, 132407 (2015).

[19] V. N. Muthukumar, R. Valenti, and C. Gros, Theory of nonreciprocal optical effects in antiferromagnets: The case of Cr_2O_3, Phys. Rev. B **54**, 433 (1996).

[20] V. V. Eremenko, Y. G. Litvinenko, N. K. Kharchenko, and V. M. Naumenko, *Magneto-Optics and Spectroscopy of Antiferromagnets* (Springer New York, 1992), p. 276.

[21] B. B. Krichevtsov, V. V. Pavlov, and R. V. Pisarev, Nonreciprocal optical effects in antiferromagnetic Cr_2O_3 subjected to electric and magnetic fields, Sov. Phys. JETP **67**, 378 (1988).

[22] R. V. Pisarev, Crystal optics of magnetoelectrics, Ferroelectrics **162**, 191 (1994).

[23] Y. R. Shen, Faraday rotation of rare-earth ions. I. Theory, Phys. Rev. **133**, A511 (1964).

[24] J. F. Dillon, Jr., H. Kamimura, and J. P. Remeika, Magneto-optical properties of ferromagnetic chromium trihalides, J. Phys. Chem. Solids **27**, 1531 (1966).

[25] T. J. Martin and J. C. Anderson, Magneto-electric annealing effects of Cr_2O_3, Phys. Lett. **11**, 109 (1964).

[26] R. V. Pisarev, B. B. Krichevtsov, and V. V. Pavlov, Optical study of the antiferromagnetic-paramagnetic phase-transition in chromium-oxide Cr_2O_3, Phase Transitions **37**, 63 (1991).

[27] Note that the representation $\alpha = \alpha_0\eta(T)\chi(T)$ is an approximation which formally allows us to express the specific EFIF as $d\Theta/dV = K[p\chi(T) + q]\eta$. We prefer Eq. (5) over the factorized representation because the former expresses the distinctly different microscopic origin of the terms $p\alpha$ and $q\eta$.

[28] M. E. Fisher, Perpendicular susceptibility of the Ising model, J. Math. Phys. (N.Y.) **4**, 124 (1963).

[29] U. Firgau, Zur theorie des ferromagnetismus und antiferromagnetismus, Ann. Phys. (Berlin) **432**, 295 (1941).

[30] P. Borisov, A. Hochstrat, V. V. Shvartsman, and W. Kleemann, Superconducting quantum interference device setup for magnetoelectric measurements, Rev. Sci. Instrum. **78**, 106105 (2007).

[31] D. S. McClure, Comparison of the crystal fields and optical spectra of Cr_2O_3 and ruby, J. Chem. Phys. **38**, 2289 (1963).

[32] W. Kaiser, S. Sugano, and D. L. Wood, Splitting of the Emission Lines of Ruby by an External Electric Field, Phys. Rev. Lett. **6**, 605 (1961).